Passive Radio Frequency Techniques & Demonstration for Space Domain Awareness

Zach Leffke, MSEE
Virginia Tech National Security Institute, Mission System Division
Kevin Schroeder, PhD
Virginia Tech National Security Institute, Mission Systems Division

Matthew Phelps, PhD
USSF Space Systems Command

Justin Fletcher
USSF Space Systems Command

ABSTRACT

Passive Radio Frequency (PRF) technology for Space Domain Awareness (SDA) has been identified in US Space Force's (USSF) Space Doctrine "Publication 3-100, Space Domain Awareness" [1] as a technology of interest to the SDA mission. Passive RF sensors utilize the signals emitted from spacecraft to determine the vehicle's position and motion which in turn can be used for orbit determination and custody maintenance. Passive RF techniques also include analysis of signal external characteristics, using both traditional signal processing and RF Machine Learning (RFML) techniques, in order to characterize the spacecraft including identification, pose estimation, pattern of life, change or event detection, intent estimation, early warning, and tipping and queuing of other sensors systems including RADAR and optical sensors. Primary advantages of passive RF include persistent observations during day and night, observation during inclement weather, and rapid revisit. This work will cover efforts at the Virginia Tech National Security Institute to develop an initial proof of concept Passive RF capability utilizing assets from the Virginia Tech Ground Station (VTGS) and relatively low cost commercial off the shelf (COTS) Software Defined Radio (SDR) technology. Current objectives of the system include tracking geosynchronous spacecraft at S-Band satellite communications frequency allocations, exploring pose estimation via polarimetric analysis of satellite downlinks, and initial data collection for exploring multiple algorithms for tracking and satellite characterization. The specific Passive RF technique being examined for this initial proof of concept is RF Interferometry which utilizes long separation, called baselines, between multiple coherent satellite receiver systems and offers potential sub-arcsecond angular resolution for tracking observations. The technical design of the real-world interferometer will be presented, including implementation challenges such as timing and synchronization between multiple sites and system calibration. Initial results of the system, derived from on air real world measurements, will also be presented concerning both satellite tracking and characterization. The paper will conclude with discussion of refinements and future work for the system, including tracking and characterization in alternative flight regimes, expanding the frequency coverage of the system and the resulting impacts to system design, and potential signal processing and RFML techniques that can be leveraged for the SDA mission and tested with the system.

1. INTRODUCTION

Passive Radio Frequency (Passive RF or PRF) technology for Space Domain Awareness (SDA) has been identified in US Space Force's (USSF) Space Doctrine "Publication 3-100, Space Domain Awareness" [1] as a technology of interest to the SDA mission. This paper will describe initial efforts by Virginia Tech's National Security Institute (VT-NSI) to develop a real-world PRF testbed for exploring multiple applications of RF sensing systems for the SDA Mission. The first algorithm explored with this testbed, and the focus of this paper, is a differential tracking interferometer with the purpose of tracking and collecting data on geosynchronous (GEO) spacecraft. A *tracking* interferometer should not be confused with a *resolving* interferometer commonly used in the radio and optical astronomy communities. Tracking

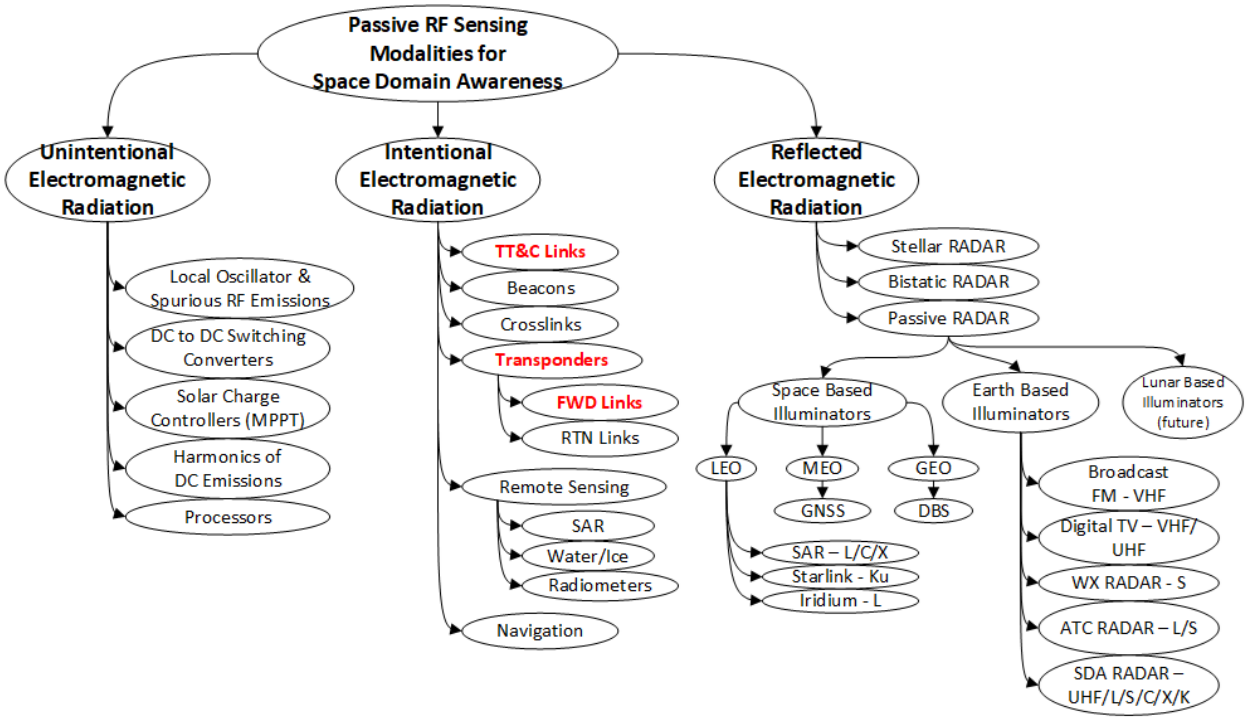

Fig. 1: Passive RF Sensing Modalities for Space Domain Awareness, red indicates the signals of interest for this paper.

interferometers require significantly shorter distances between the receiving systems (See Section 2.1.2). The primary objective of the tracking interferometer discussed in this work is to provide tracking data on par with current optical system data quality. The second objective of this effort is to collect RF data that can also be utilized for satellite characterization purposes. The theory, technical implementation, deployment, and initial results from real-world on air observations of the differential tracking interferometer will be discussed in detail in this paper.

Fig. 1 shows the sensing modalities for Passive RF. There are three general categories by which an orbiting object may radiate electromagnetic energy in the RF spectrum: unintentional, intentional, and reflected. This paper focuses on the intentional radiation from Tracking, Telemetry, & Control (TT&C) downlink signals as well as forward downlink (gateway to user) signals, called out in red in the figure. Unintentional electromagnetic radiation is the radiated energy that is produced by onboard electronic or RF subsystems and is accidentally radiated or leaked from the space vehicle. Reflected electromagnetic energy is the mechanism by which active systems, such as RADAR or LiDAR, operate and is useful for tracking targets that do not inherently carry functioning electronic or RF systems, such as debris and defunct spacecraft. These same reflected signals may be used by Passive RF systems operating in collaboration with or independent of the radiation source.

Passive RF sensors utilize the signals radiated from spacecraft to determine the vehicle's position and motion which in turn can be used for orbit determination and custody maintenance. Passive RF techniques also include analysis of signal external characteristics, using both traditional signal processing and Radio Frequency Machine Learning (RFML) techniques, in order to characterize the spacecraft including identification, pose estimation, pattern of life, change or event detection, intent estimation, early warning, and tipping and queuing of other sensors systems including RADAR and optical sensors.

Passive RF techniques yield additional information that can be utilized independently or through data fusion techniques with optical and RADAR data. It is important to note that Passive RF techniques are not a replacement for existing optical and RADAR systems and are envisioned to compliment existing SDA techniques. Primary advantages of Passive RF include persistent observations during day and night, observation during inclement weather, and rapid revisit. Passive RF techniques offer the possibility of low cost systems capable of providing useful SDA data. Due to the potential for relatively low cost systems, it is possible to proliferate PRF sensors in order to increase coverage

and generate data useful to the SDA mission. This is similar to the concept of proliferating multiple small aperture optical systems for SDA applications. Optical system costs goes as $\sim D^3$, D being aperture diameter [2]. Robust RF systems have been developed for over a century with deployment into nearly all environments on and around Earth. With the constant evolution of RF hardware technology, manufacturing costs tend to decline as the industry matures. Technologies such as software radio, RFML & AI/ML techniques, and RF device manufacturing along with open source signal processing libraries such as GNU Radio[3] and liquid-dsp[4], offer the ability for low cost systems to be developed rapidly. Maintenance costs may be lower than optical as well given the lack of fragile optics with Passive RF.

Additional benefits that come from 24/7/365 observation is the ability to collect data relevant to Machine Learning (ML) techniques for satellite characterization purposes. One of the major challenges with ML techniques is the ability to collect sufficient training data, with proper data labelling, for the multitude of algorithms. A common method for generating training data is the utilization of high fidelity models to generate synthetic data. A shortcoming of this method is that the synthetic data may not truly represent the target system and real-world observation environment and thus potentially incorrectly trains the ML algorithms. Collection of real-world data is ideal for training purposes, but can be very costly and time consuming. In the domain of RFML it has been demonstrated that it is possible to combine a small amount of real-world data with synthetically generated data to increase the performance of RFML methods[5].

An obvious shortcoming of Passive RF is the possibility that a system may cease to emit for sensors relying on intentional radiation from the vehicle. This may occur for a number of reasons, such as the decommissioning of a spacecraft and its relocation to a disposal orbit. Similarly, debris in orbit does not intentionally emit RF signals and are not trackable with the same techniques needed for systems that are intentionally radiating. This is somewhat mitigated by alternative PRF techniques that make use of reflected electromagnetic radiation, (e.g. Passive RADAR), or make use of the reception of unintentional radiation, but discussions of those techniques are out of scope for this paper.

2. THEORY

This section describes the fundamentals of interferometry and polarimetry. Both subjects are too in depth to fully cover in this paper and full treatment of the topics can be found in the references. This section seeks to summarize the key equations and design considerations to provide a basic understanding of the concepts as they relate to the SDA mission.

2.1 Interferometry

Interferometry is an established tool used by both optical and radio astronomers. The primary benefit of interferometry is a dramatic increase in the resolution of observing instrumentation. The basic concept involves combining light (or any EM wave) to produce alternating sequences of light and dark bands, called fringes or the fringe pattern. These alternating bands are produced due to the constructive and destructive interference of radiation, hence the term *interferometer*. Analysis of the fringe pattern can yield very high resolution angular measurements. The resolution of an interferometer is inversely related to the spatial separation of the receiving systems relative to the wavelength under observation (see Equation 2). Increasing the spatial separation of, or distance between, the receiving elements of an interferometer serves to produce finer resolution. We conclude this introduction to Section 2.1 with a reminder concerning the terms *resolution* and *accuracy*. In simple terms, resolution is the smallest amount of change that can be measured, while accuracy is how close a measurement is to the true value. Section 2.1.2 seeks to address the resolution of the system and show how the ability to detect sub-arcsecond changes is possible. Section 2.1.3 seeks to address the accuracy of the system and shows a technique for mapping the high resolution measurements to the real world.

2.1.1 Basic Radio Interferometer Description

Fig. 2 depicts a simple two element radio interferometer and introduces the basic parameters used to define and analyze the interferometer. For this paper and demonstration some key assumptions are made. First, it is assumed that the receiving elements are far enough from the inherently spherically radiating source of emission that the incident field can be considered a planar wavefront, and when considering two elements of the interferometer there exists a line of equal phase along the planar wavefront. Second, the source of the emission is considered monochromatic in nature, simplifying the mathematics, and a valid assumption as demonstrated in Section 5.

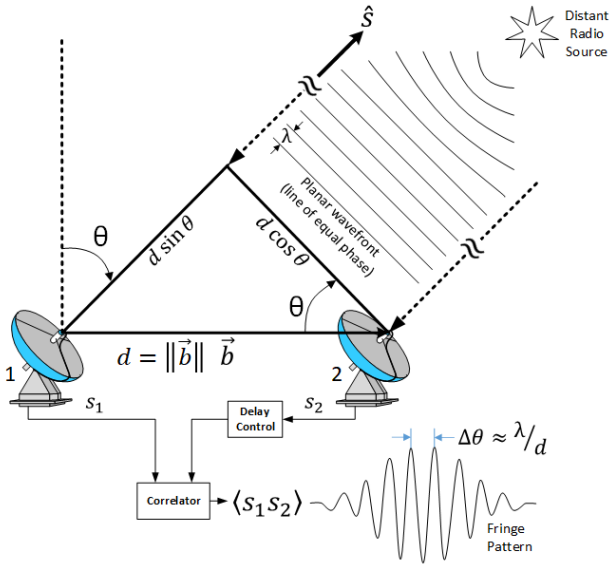

Fig. 2: Graphical depiction of a single baseline, two dimensional, idealized radio interferometer.

The vector $\hat{S}$ is a unit vector that points from the interferometer to the distant radio source, and while the figure shows it originating from antenna 1, practically $\hat{S}$ can originate at any point along the baseline vector between antenna 1 and antenna 2 so long as $d <<$ distance to the target. For the tracking problem, the goal is to determine this vector or equivalently the associated angles in a relevant coordinate system, such as azimuth and elevation in the South-East-Zenith (SEZ) frame. A baseline is the vector, $\overrightarrow{b}$, connecting the reference points of two antennas. The distance between the two antennas is the magnitude of the baseline, $d = \| \overrightarrow{b} \|$. The radio source is located at an angle θ off of the line orthogonal to the baseline.

Consider a distant radiating source emitting monochromatic radiation such that a planar wavefront is incident upon the elements (antennas) of an interferometer. In Fig. 2 the wavefront arrives first at antenna 2 then must travel an additional distance of $dsin\theta$ to arrive at antenna 1. The amount of time required to traverse this distance is inversely proportional to speed of light, c. Depending on the wavelength of the electromagnetic wave, λ [m], multiple cycles of the wave may be required before the distance $dsin\theta$ is traversed. The phase of the signal changes by 2π radians for every cycle of the wave. A phase shift between the signals produced by the receivers, S_1 & S_2, is thus introduced but with a potential ambiguity of 2π radians. The phase shift produced at antenna 1 relative to antenna 2 is given by:

$$\tau_{12} = \frac{2\pi}{\lambda} d \sin\theta \tag{1}$$

Where τ_{12} is the *interferometric phase*, measured in radians, at antenna number 1 referenced to antenna number 2, θ is the angle measured from the line orthogonal to the baseline in radians, λ is the wavelength of the wave in meters, and d is the baseline distance in meters between the two receiving antennas. Note that the $2\pi/\lambda$ term is often referred to as the *wavenumber* and represented by the variable k or β in many electromagnetics references. It is useful to think of the wavenumber quantity in terms of its units, radians per meter, which shows the phase rotation as the wave travels in the spatial domain. Equation 1 is the foundation upon which the interferometer is constructed.

The two antenna interferometer discussed here can only yield a single angle of interest, i.e. azimuth or elevation. In order to determine both angles, a second baseline is needed, thus requiring at least one more antenna and the associated receiving electronics. Depending on antenna geometry, often constrained by installation site requirements, it is usually required to compute a projected baseline, also known as an effective baseline. This is because the baseline vector of a given pair of antennas in an interferometer is often not physically orthogonal to the observed region of the sky, i.e. the ideal orbit slot location in 3D space for a GEO spacecraft. It has been shown that three antennas with generic orientation to each other are sufficient and can be mapped to azimuth and elevation measurement with high precision [6] so long as the projected baselines are far enough apart to meet resolution requirements.

2.1.2 Resolving vs. Tracking Interferometers

It is important to note the difference between traditional radio astronomy interferometers and the type of interferometer developed for this SDA proof of concept. Traditional radio interferometers are typically interested in mapping the spatial structure of distant sources of electromagnetic emissions. This implies that the target is not a point source, but is emitting electromagnetic radiation across a relatively large angular spread. A high resolution interferometer is needed in order to discern the spatial structure of the target, which we will refer to as a *resolving* interferometer, because the emission source is producing radiation on the same frequency (or wavelength) across the full angular spread. Equation 2 shows the traditional definition of the resolution of an interferometer [7]:

$$\Delta\theta \approx \frac{\lambda}{d}[radians] \tag{2}$$

where $\Delta\theta$ is the resolution of the interferometer in radians, d is the distance between the two observing antennas in meters, and λ is the wavelength of the electromagnetic radiation in meters. As shown in the equation, as the baseline, d, increases the resolution of the interferometer decreases (finer resolution).

For the SDA mission, the conditions are different. Each spacecraft of interest can be considered to be a point source of electromagnetic radiation originating from its downlink antenna. We are not interested in mapping the spatial structure of the spacecraft, and therefore we do not require the same type of resolving interferometer.Instead we are interested in utilizing the interferometric phase information in order to track the spacecraft position and velocity. This type of interferometer we will refer to as a *tracking* interferometer and this is the type developed for the VT-NSI PRF testbed. While the basic electromagnetic and signal processing principles apply to both, with interferometric phase being the primary measurement quantity of interest, the two systems are significantly different.

The main difference between a resolving and tracking interferometer is the required spatial separation (baselines) between the antennas. The required spatial separation for a resolving interferometer is much higher than that required for a tracking interferometer. This is perhaps best highlighted with an example. The target resolution of the SDA tracking interferometer is 1 arcsecond or 0.000278 degrees. S-Band downlink signals have a wavelength of about 0.130 meters. Rearranging Eq. 2 and using $\Delta\theta = 1$ [arcsec] $= 4.484814x10^{-6}$ [rad] and $\lambda = 0.130$ [m] we have: $d = 2.681442$ [km]. Thus a resolving interferometer would require more than 2.681 kilometers of spatial separation between antennas to achieve less than 1 arcsecond of resolution in the satellite S-Band frequency allocations. For the SDA mission, this would only be useful if the targets were 1 arcsecond apart and transmitting on the exact same frequency. On the other hand, for a tracking interferometer, if we rearrange Eq. 1 to solve for θ we have:

$$\theta = \sin^{-1}\left(\frac{\lambda\,\tau_{12}}{2\pi d}\right) \tag{3}$$

In Fig. 3 we plot θ for the common satellite communications frequency allocations for a range of baselines from 1 meter to 100 kilometers, keeping in mind the target of 1.0 arcseconds of relative angular motion as the required resolution of the interferometer. We assume a detection threshold of $\tau_{12} = 2$ [deg] as a conservative value that is detectable in the signal processing chain. We see from Fig. 3, for S-Band satellite communications frequency (yellow line) that the required baseline for $\theta = 1$ arcsecond of relative motion is approximately 150 meters. Stated another way, with 150 meters of spatial separation between antennas, 1 arcsecond of relative motion will produce 2 degrees of interferometric phase shift which easily detectable in the signal processing domain. A spatial separation of 150 meters for a tracking interferometer is significantly less than the required 2.68 kilometers of spatial separation required for a resolving interferometer. This dramatically relaxes the implementation requirements for the tracking interferometer, while meeting the goals of the SDA mission.

2.1.3 Differential Tracking

In order for an interferometer to function properly, the receiving stations must operate coherently. For the purposes of this paper, this means that each receiving node (antenna, downconverter if used, receiver, etc.) must be aligned in frequency, phase, and time to every other receiving node in the interferometer network. For Very Long Baseline Interferometry (VLBI) in radio astronomy, from which we take inspiration for this work, the spatial separation of the observatories is so long, often spanning multiple continents and potentially including orbiting platforms, that the

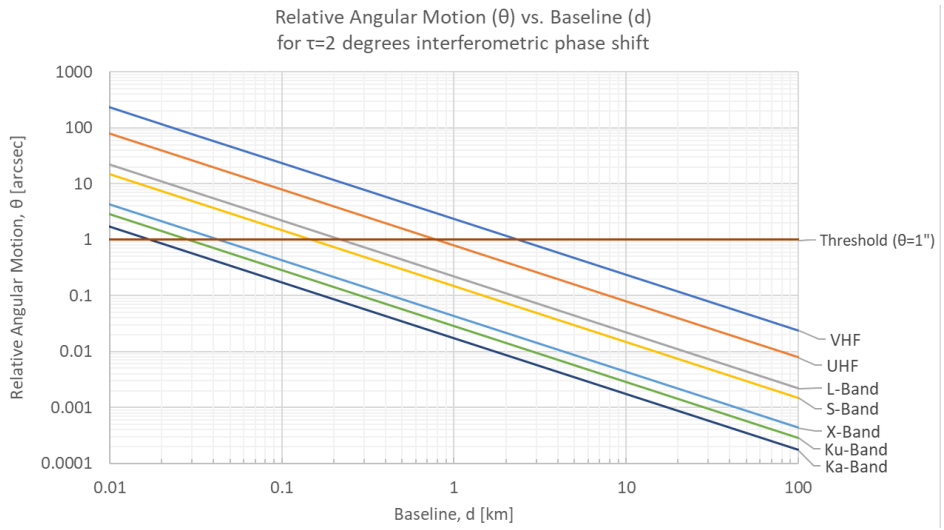

Fig. 3: Relative Angular Motion, θ, vs. Baseline, d, for interferometric phase detection threshold of $\tau_{12} = 2[deg]$.

systems cannot be practically connected to each other for the purposes of cohering them. In the VLBI scenario, the observing stations first observe a known emission source such as a pulsar simultaneously at all receiving stations. They then turn to observing the signal of interest from the target emission source.When the recorded RF data is brought together at the central processing facility, the initially observed known emission source is used to cohere the received signals, aligning them in frequency, phase, and time. After initial alignment, the signals are then processed using the correlator to produce the desired interferometric data. This 'align first, correlate second' approach is made possible due to the ultra-high stability of the clocks located at each observatory, typically hydrogen MASERS, keeping the datasets coherent during the observation windows which can last many hours. Without access to the ultra-stable clocks, each observatory would have to periodically observe the known emission source and then return to observing the signal of interest, thus reducing the amount of time to collect useful information on the signal of interest.

For the VT-NSI interferometer, time and budget restrictions did not allow for full scale synchronization (time, frequency, and phase), nor the acquisition of expensive ultra-stable clocks such as Hydrogen MASERs. This however is not considered a deficiency in the system as one of the major objectives of this effort is maintain a low-cost approach and test various algorithms that do not require expensive subsystems. Instead, an external calibration signal, referred to as a reference signal, is used to cohere the spatially separated receivers, and in this proof of concept that reference signal is supplied from another geosynchronous spacecraft. This is similar to the concept for VLBI mentioned above, where there is a known emission source and a target emission source, with one significant difference: the reference signal and the target signal are observed *simultaneously*. This technique is called *differential tracking interferometry* and is extensively described by Kawase et al in [8] and [6]. We have slightly updated the description of it, and use modern software radio technology to implement it, but the fundamental concept remains the same.

A key feature of this technique is the use of a known reference signal from another spacecraft in GEO. This type of tracking is useful in commercial satellite operations where multiple satellites may be in close proximity to each through assignment to the same orbital slot. The top portion of Fig. 4 shows a block diagram version of the tracking interferometer signal processing, capable of producing an interferometric phase shift that can be mapped to the change in angular separation of the spacecraft under observation (resolution). The tracking interferometer is cable of showing the change in angular separation of the two spacecraft (resolution), but not necessarily the true absolute position of the spacecraft (accuracy). For this, the bottom half of Fig. 4 is required. This portion of the system relies on accurate knowledge of the location and orbit of the reference spacecraft. This can be obtained through a combination of techniques such as optical observation, RADAR, or cooperatively with the satellite owner using ranging transponders or GPS receivers onboard the spacecraft. The orbit of the target spacecraft is then determined *relative* to the reference spacecraft. Thus the accuracy of orbit determination (OD) solution for the target spacecraft is driven by the accuracy of the knowledge of the reference spacecraft orbit. Finally, it should be noted that while this technique is effectively taking two angular measurements (azimuth and elevation) when combined with the knowledge of the reference satellite orbit,

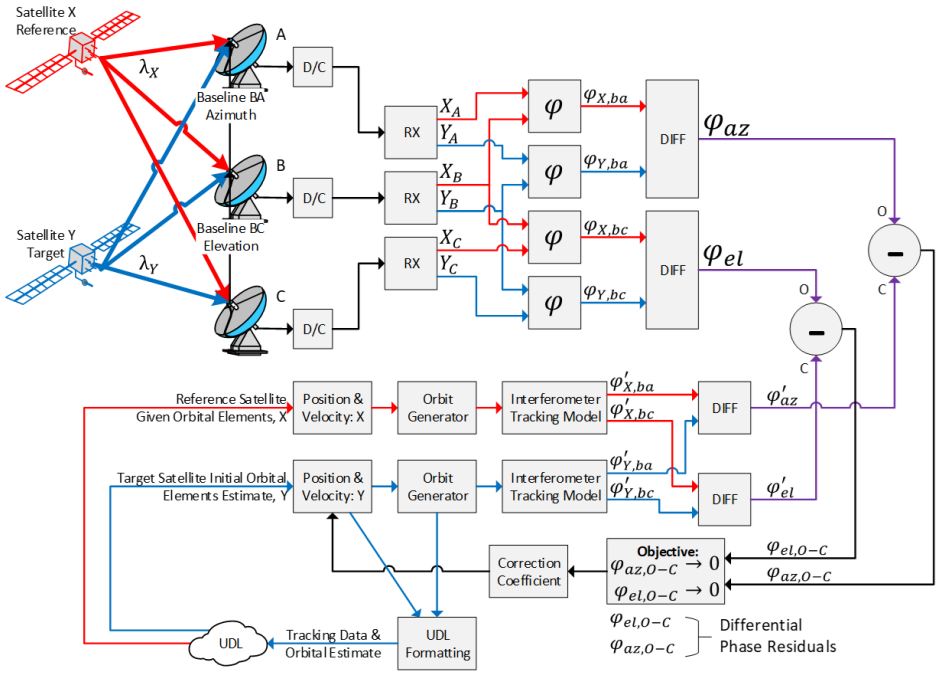

Fig. 4: Differential Tracking Interferometer.

it is possible to yield a full orbital solution for the target satellite, though does not make use of traditional angles-only OD techniques.

2.2 Polarimetry

Polarimetric observation of RF signals emitted from spacecraft offers the potential to provide useful information for satellite characterization. For a thorough treatment of polarization topics for RF systems the reader is encouraged to see [9].The orientation of the electric field component defines the polarization of the wave, per IEEE standard. Any polarization state can be defined in terms of orthogonal linear components, x and y in our example, and critical for our SDA oriented mission, any polarization state can be *measured* using dual orthogonal linear antennas.

2.2.1 Polarimetry for SDA

Many circularly polarized antenna systems, common in satellite systems, do not produce pure circular polarization in all directions. Typically these antenna systems are optimized to produce circular polarization along the boresight vector of the antenna, which is usually the direction of maximum gain and the direction the radiation is intended to propagate. As one moves away from the boresight vector, the circularity of the wave degrades and appears to a distant observer to be more elliptical. Thus it is feasible that monitoring of the polarization state of a downlink signal could yield information concerning the pose or attitude of a spacecraft. If for example the spacecraft maneuvers to orient a payload in a specific direction, the polarization state of the downlink signals from the spacecraft may also change. Monitoring this over a long period of time may indicate patterns of life as well in the pose of the spacecraft. Finally, observation from multiple viewing angles of the polarization state of the spacecraft downlinks, as well as multi-frequency observations if the spacecraft operates in multiple bands, may allow for the determination of the specific direction in which the spacecraft oriented itself.

2.2.2 Polarization State & Measurement

Fig. 5 (left) shows the definition of the Polarization Ellipse, which can be thought of as tracing out the tip of a rotating electric field vector as it rotates around the axis of propagation (out of the page). This is used to define some key

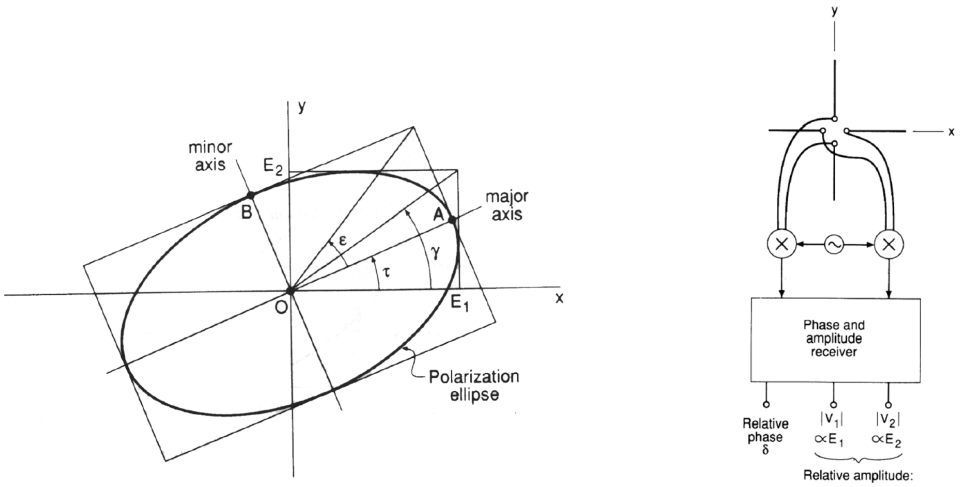

Fig. 5: The Polarization Ellipse (left) and model polarimeter (right), both taken from [9].

variables used in the mathematical description of electromagnetic wave polarization states. The polarization state of a wave can be sufficiently defined by two variables: (γ, δ) or (ε, τ). These two sets of variables have their own uses, and can be defined in terms of one of another. The τ variable for example is useful in defining the orientation of the major axis of the ellipse, whereas the ε variable is useful for determining the axial ratio of the wave. The (γ, δ) set of variables lends itself well to direct measurement using a polarimeter discussed below. Not depicted in Fig. 5 (left) is the δ variable which is the relative phase between the x and y components of the E-field.

Fig. 5 (right) shows a model for an ideal polarimeter. Any polarization state can be measured using dual orthogonal linear antennas using a coherent receiver so that the relative phase between the components, δ, can also be measured. The receivers used in the differential tracking interferometer meet these requirements with antenna feed assemblies that use dual orthogonal linear elements and dual coherent receive chains. Thus any antenna in the interferometer also serves as a polarimeter. This is useful for matching the polarization sense of the incoming wave to maximize Signal to Noise ratio, and as a by product the polarimetric measurements can be used for satellite characterization and event detection. The following equations define the parameters of interest mathematically which is reflected in Section 3.3.2. We begin with the definition of γ:

$$\gamma = \tan^{-1}\left(\frac{E_y}{E_x}\right), \ 0^\circ \leq \gamma \leq 90^\circ \tag{4}$$

Where E_y and E_x are proportional to the magnitudes of the complex voltages produced by the receiver. Practically speaking, when implementing in signal processing, the ATAN2 function should be utilized, and the magnitude of the complex IQ data stream can be used to compute the relative field magnitudes (See Section 3.3.2).

The relative phase, δ, between the orthogonal components can be measured directly using Fast Fourier Transform (FFT) techniques, just like the interferometric phase. This process is describe in detail in Section 3.3.1. The range of δ is $-90^\circ \leq \delta \leq +90^\circ$, where positive indicates left handedness and negative indicates right handedness.

With a method for measuring the (γ, δ) set we can define the method for determining the other variables of interest.

$$\varepsilon = \frac{1}{2}\sin^{-1}(\sin 2\gamma \sin \delta), \ -45^\circ \leq \varepsilon \leq +45^\circ \tag{5}$$

$$\tau = \frac{1}{2}\tan^{-1}\left[\frac{\sin 2\gamma \cos \delta}{\cos 2\gamma}\right], \ 0^\circ \leq \tau \leq 180^\circ \tag{6}$$

It should be noted that τ in Equation 6 used for polarimetry and common in EM references is not the same as the τ_{12} used in the interferometry discussion. Finally, we have the following definition for *axial ratio*:

$$R = -\cot \varepsilon \tag{7}$$

Before continuing, it should be noted that the antennas used in this proof of concept effort are prime focus parabolic *reflector* antennas. When a circularly polarized electromagnetic wave reflects off an interface, it flips polarization

sense. Hence a Right Hand Circularly Polarized (RHCP) signal when measured with a prime focus parabolic reflector antenna will be detected as a Left Hand Circularly Polarized (LHCP) wave. This flip in polarization sense is accounted for in the signal processing software utilized for the proof of concept.

3. SYSTEM IMPLEMENTATION

3.1 Overview

The overall objective of this proof of concept is to develop a differential tracking interferometer and obtain on air real-world measurements. A goal of relatively low-cost implementation is desirable. The satellite communications band of interest is S-Band at 2200 MHz to 2400 MHz. This band was selected for a number of reasons. First, it is within the reception range of the N310 Universal Software Radio Peripherals from Ettus Research. This means that no down conversion devices, such as low noise block down converters, are required which simplifies the implementation. Second is that spacecraft in multiple flight regimes utilize S-Band allocations including LEO, MEO, HEO, GEO, Earth-Sun L1, Earth-Sun L2, and the Lunar Reconnaissance Orbiter (LRO) in orbit arond the moon. This offers a target rich environment for experimentation which is ideal for a passive RF testbed for SDA applications.

3.2 Ground Station Design

Assets provided by the Virginia Tech Ground Station (VTGS) included three tracking station locations with available prime focus parabolic reflector antennas, the VTGS signal processing servers, and the VTGS Core Network and Virtual Private Network infrastructure for the SDA project which links the three tracking stations together with the core network. KBR provided three dual orthogonal linear polarization (X/Y) S-band feed assemblies from Alaris mWave, high-Q S-Band filters and Bias-Ts from Mini-Circuits, high quality S-Band low noise amplifiers from Alaris Kuhne and weatherproof enclosures from L-Com. VT-NSI supplied the remaining equipment including high quality Trimble Thunderbolt-E GPS Disciplined Oscillators (GPSDOs), power supplies, and miscellaneous wiring and electronics.

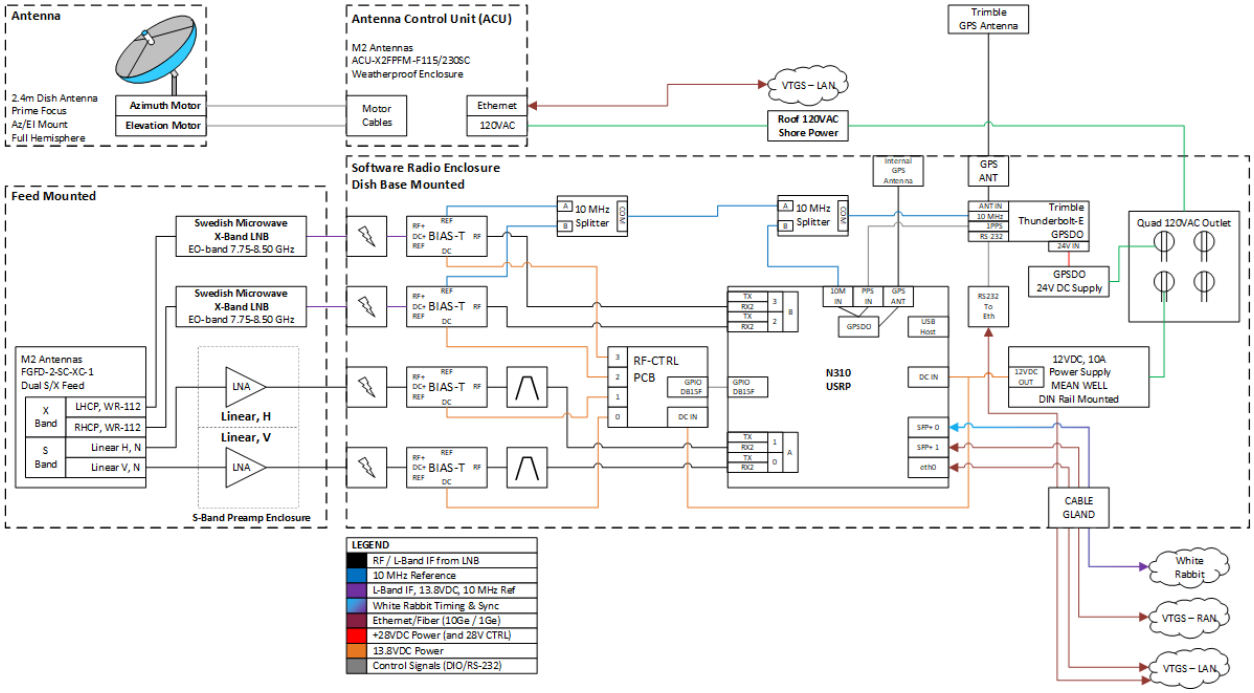

Fig. 6: RB1311 Ground Station, Interferometer RF Node.

Figure 6 shows the hardware block diagram of the ground station for the RB1311 location, VT-NSI's primary building which also house VT-NSI's SDA Telescope system. The other two ground stations are referred to as the NIS Tracking Station (NISTS) and the Prices Fork Tracking Station (PFTS) systems with approximately 512 meters and 3.14 kilometers as the baseline distances to RB1311, respectively. Their ground station design is nearly identical with the

notable exception that the RB1311 antenna feed assembly is dual-band and capable of X-Band downlink reception as well. It was decided to retain this capability for future expansion into other frequency bands of interest.

The core of the ground station design is centered around the Ettus Research N310 Universal Software Radio Peripheral (USRP). This software radio converts the analog RF signal into a stream of digital in-phase and quadrature (IQ) samples. Each radio contains 4 coherent receive chains, important for the polarimetry portion of the project when combined with the dual orthogonal linear feed assemblies. The N310 reception range is 10 MHz to 6 GHz and thus is capable of S-Band reception at 2.2 to 2.4 GHz without the need for additional downconverters in the RF front end receive chain. The N310s can support approximately 100 MHz of instantaneous bandwidth over 10 gigabit per second ethernet links. The N310s natively support the White Rabbit Timing and Synchronization protocol which can enable sub-nanosecond timing and synchronization in multi-USRP deployments [10]. White Rabbit is not currently deployed in the VT-NSI PRF testbed, nor is necessary for the differential tracking interferometer, but is expected to be in the near future to test other algorithms of interest for the SDA mission.

3.3 Signal Processing

The primary signal processing framework utilized for this proof of concept is the open source GNU Radio framework[3]. A flowgraph is a sequence of digital signal processing blocks that are connected in such a way as to process a stream of digital samples. GNU Radio also allows for the creating of custom signal processing blocks in what are referred to as Out-Of-Tree Modules (OOTMs). The main OOTM utilized on this project is the Signal Metadata Format (SigMF) [11] source and sink blocks. SigMF is an open specification for recording digital streams of data and retaining key metadata in JSON. The metadata contains information such as timestamp, tuned center frequency, sample rate, and sample data type. Additional custom metadata can be inserted in a number of ways and specified via the extensions, such as which satellite systems are under observation and associated information, which ground station is recording the data along with its position info (lat/lon/alt or ECEF), polarimetry information, etc. SigMF is used on this program for both raw IQ data recording (in complex format) as well as digital data products (in float format), such as polarimetry measurements, frequency offset (doppler) measurements, and the interferometric phase data.

The figures presented in this section are from the flowgraphs developed for this proof of concept. The full flowgraphs are too large to include in this paper, but selected flowgraph sections are included to show certain functionality key to this program for interferometry (tracking) and polarimetry (satellite characterization). The full set of flowgraphs, hierarchical flowgraphs, and custom processing blocks and OOTMs developed for this project will be posted to the VTGS's public github page [12].

3.3.1 Interferometry Flowgraphs

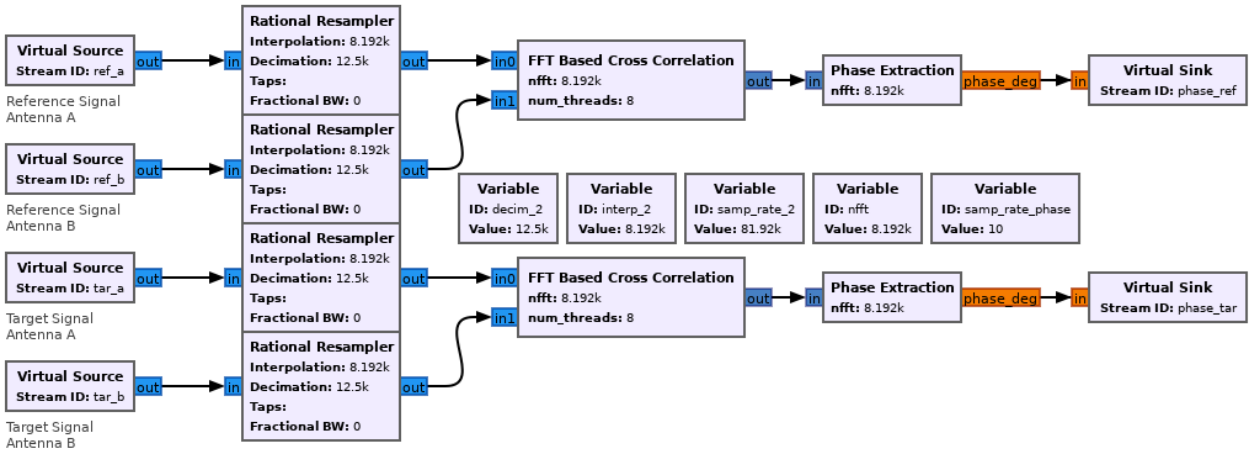

Fig. 7: Interferometric phase measurement using the Fast Fourier Transform (FFT) based cross correlation technique.

Figure 7 shows the primary method for interferometric phase measurement in GNU Radio using a combination of Fast Fourier Transform (FFT) based cross correlation and then a phase extraction block. The figure depicts the implemen-

tation in the differential tracking interferometer flowgraph, thus there are two measurements being obtained for a the single baseline, one measurement of the reference satellite signal and one measurement of the target satellite signal. In the current implementation the final output sample rate is 10 phase measurements per second. In fact both the FFT Cross Correlation block and the Phase Extraction block are custom hierarchical blocks, and contain more signal processing steps within them.

3.3.2 Polarimetry

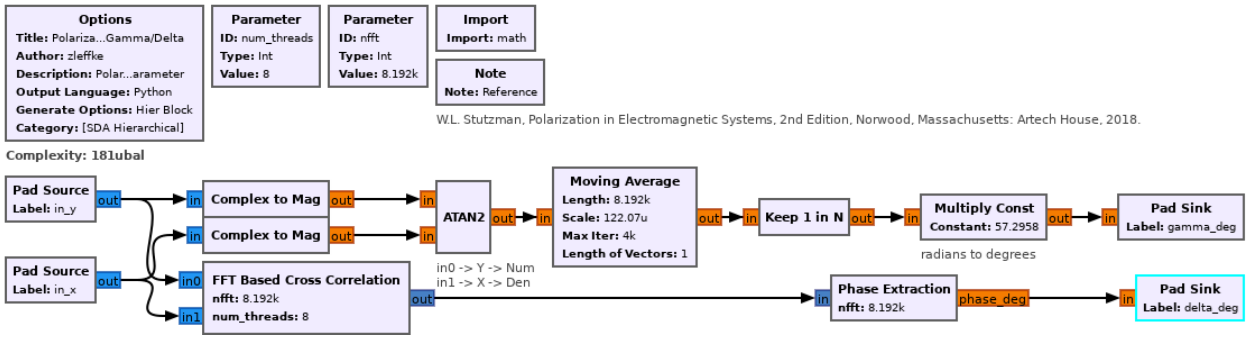

Fig. 8: Example polarimetry hierarchical flowgraph, γ, δ measurement technique.

Figure 8 show the GNU radio hierarchical flowgraph used to measure the (γ, δ) polarization parameters. Note that the method for measuring the relative phase, δ, is exactly the same as the method for measuring interferometric phase. The (ε, τ), axial ratio, and polarization ratio, and polarization ellipse representation are also computed in the flowgraph but are not depicted here.

3.4 Data Processing Pipeline

Figure 9 shows the current data pipeline for this proof of concept. Currently this pipeline is executed periodically at a predefined cadence, such as 1 minute recordings every 10 minutes. The raw IQ samples for the dual orthogonal linear elements are collected on the local ground station radio server. We then proceed to run the polarization flowgraph to match the right handed polarization sense of the Sirius-XM TT&C signals to maximize their Signal to Noise Ratio (SNR). We do this for both the target and reference signal, with the output again being raw IQ samples. We also save off the polarimetric measurement data in the same flowgraph. We then use the File Transfer Protocol (FTP) protocol to transfer the snapshot data to the core network's Network Attached Storage (NAS) server via the VTGS VPN infrastructure. This process is executed on both ground stations simultaneously.

Within the core network, we detect the presence of ingested data and proceed with execution of the interferometric phase measurement flowgraph. Using the precise timestamp metadata in the SigMF JSON files, obtained from the high quality Trimble Thunderbolt-E GPSDOs, we first align the sample streams of the flowgraphs in time. In the same flowgraph we also measure the carrier frequency offset (CFO) of the signals of interest and save this as an additional data product. We then post these results back to the NAS, again using FTP, for backup purposes. We then execute Python based scripts for determining the differential phase measurements, the projection of the baselines of the interferometer, and the mapping of the phase results to angular measurements. We also execute satellite characterization operations, such as analysis of the carrier frequency offset measurements, which are essentially Doppler shift measurements and lead to range-rate information about the satellite motion. Any instantaneous change in the range-rate information could lead to detection of events of interest, such as the ignition of a thruster on the spacecraft. The polarization analysis is conducted to determine if any changes have occurred in the pattern of life and thus potential events of interest, such as a potential change in attitude. Finally we show an envisioned future analysis process whereby RFML and AI/ML algorithms may be applied to the raw IQ data along with the collected measurements of carrier frequency offset and polarimetric measurements.

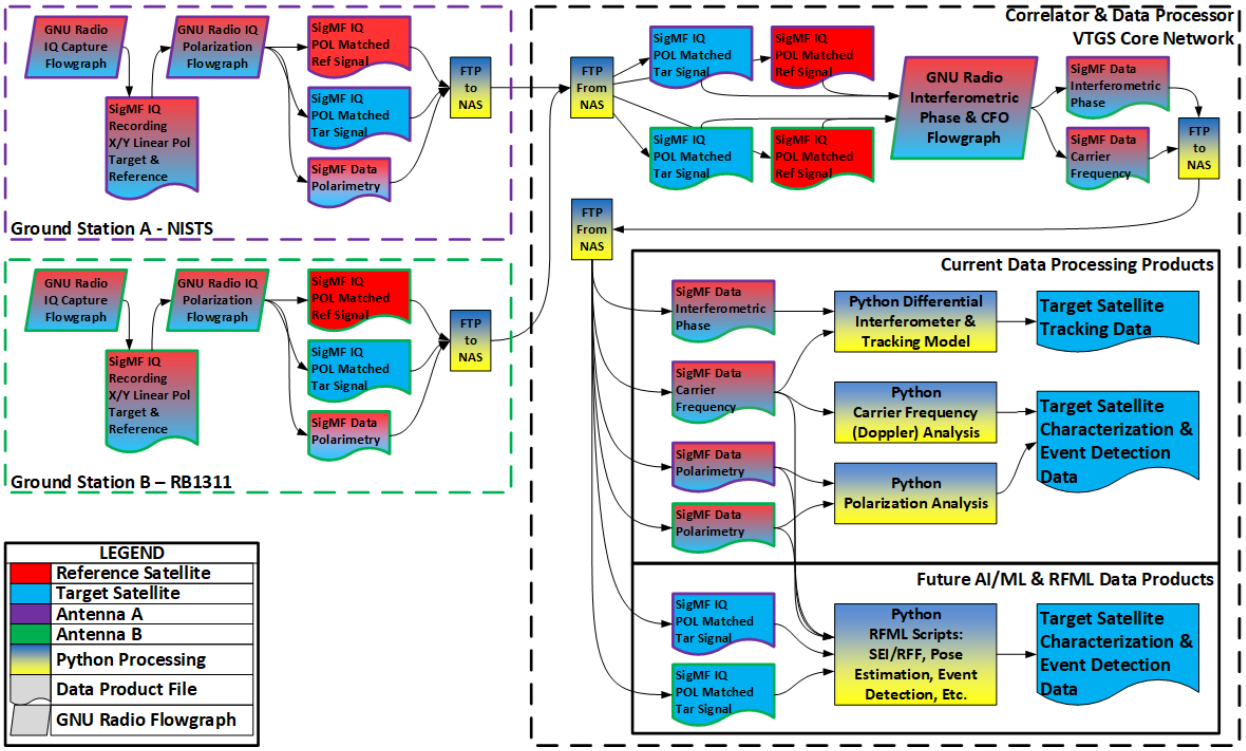

Fig. 9: Data Processing Pipeline, Ground Station to Core Network Pipeline.

4. PROOF-OF-CONCEPT DEMONSTRATION

4.1 Demonstration Objectives

A primary goal of this effort is to develop a system capable of real-world on air RF measurements with relevance to the SDA mission. To this end a number of high level objectives for a real-world demonstration of the proof of concept (POC) have been identified and are described in this section. The chosen orbital flight regime for the demonstration is Geosynchronous (GEO) orbit. Demonstration of the ability to track spacecraft in GEO using passive RF techniques with a precision and accuracy on par with optical measurements. Our target resolution is 1 arcsecond or better in angle. Relative low cost is another goal, meaning exquisite equipment is not desirable. Ability to collect data and metadata relevant to satellite characterization, event detection, pose estimation, etc. in addition to the tracking demonstration. Get on sky in a relatively short timeline of approximately 9 months.

The overall algorithm selected for the demonstration is a differential tracking interferometer which offers the possibility of sub-arcsecond tracking capability, without requiring exquisite solutions for cohering the receivers. A requirement of this technique is that at least two separate spacecraft must be within the field of view of the receiving antenna beamwidths, with one a known or trusted reference spacecraft and the other(s) the target spacecraft. The commercial S-Band frequency allocations have been chosen in part to reduce hardware complexity of the system and thus reduce overall cost, though the algorithm is applicable across all satellite communications bands, including multi-band variants. The antenna systems available to the VTGS system are also suitable for the POC, with relatively minor feed assembly upgrades and with baselines that meet the goals for tracking accuracy (in excess of 150 meters, required for sub-arcsecond capability). Finally, the selected spacecraft for the demonstration are part of the the Sirius-XM Satellite Digital Audio Radio Service (SDARS) Constellation.

4.2 Sirius-XM Overview

Sirius-XM is an American broadcast service that transmits digital audio to millions of customers via a fleet of spacecraft in geosynchronous orbit. Sirius-XM operates three spacecraft at the 85.15° West Longitude orbital slot; XM-3, SXM-7, SXM-8, which are the primary focus for the demonstration. These three satellites all operate inside a bound-

ing box centered on their orbital slot assignment and are allowed motion in longitude of ±0.1 degrees and motion in latitude of ± 0.05 degrees. Sirius-XM has been assigned frequencies in the Commercial S-Band frequency allocations of 2.319 GHz to 2.343 MHz.

XM-3 is a second generation spacecraft, was launched in February of 2005, and is built on Boeing BSS-702 bus. SXM-7 and SXM-8 are third generation spacecraft, built on the Space Systems Loral / Maxar SSL-1300 bus. SXM-7 was launched in December of 2020, and shortly after reaching orbit experienced some type of failure and was eventually declared a total loss by Sirius-XM. Though a total loss to the company, the spacecraft is nevertheless transmitting TT&C signals and is able to maintain its station keeping capability. SXM-8 was launched in June of 2021 and is the replacement for the failed SXM-7. Both SXM-7 and SXM-8 also may be using coherent ranging techniques with the newer generation RF subsystems, which is discussed in more detail in Section 5.2.1.

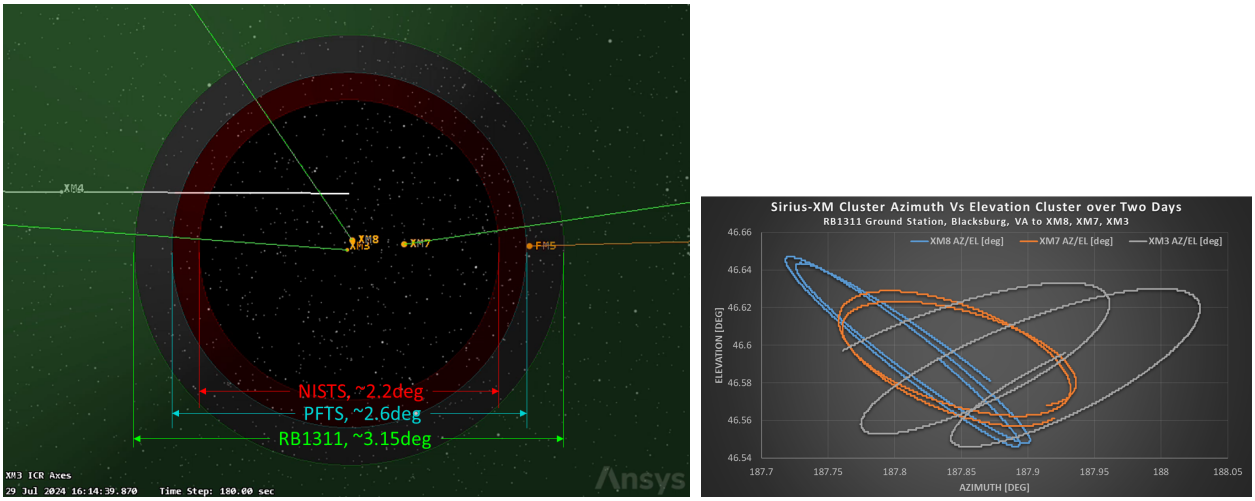

Fig. 10: (Left) Sirius-XM Cluster at 85.15°W Longitude with the VT-NSI differential tracking interferometer antenna 3dB beamwidths overlaid. (Right) Azimuth/Elevation Bounds from Blacksburg, VA.

Figure 10 (left) shows an STK simulation of the Sirius-XM cluster with the 3dB beamwidth of the VT-NSI differential tracking interferometer antenna elements overlaid. The three tracking stations involved are all located in Blacksburg, Virginia at sites on or adjacent to the Virginia Tech main campus. These tracking stations are referred to as: NISTS, PFTS, and, RB1311 and each has a receiving system as described in Section 3.2. One notable difference is the size of the parabolic reflectors at these locations: 3.6m at NISTS, 3.0m at PFTS, and 2.4m at RB1311. Antenna beamwidth, specified as the 3 dB beamwidth, decreases as antenna diameter increases, thus the concentric rings in Figure 10. The right sub-figure of Figure 10 is an elevation vs. azimuth plot showing that the spacecraft are staying within their bounding box as viewed from Blacksburg, VA.

4.3 Sirius-XM Frequency & Polarization

A key need for this demonstration is an understanding of the center frequencies of the individual spacecraft. A thorough search was conducted of open source and public information, including FCC databases. Each Sirius-XM satellite is assigned four frequencies for Tracking, Telemetry, & Control (TT&C). Figure 11 shows the individual assignment for every satellite in the constellation, with the color coded frequencies being the ones of interest for the POC demonstration.

The Sirius-XM spacecraft employ polarization diversity techniques with dual orthogonal circular polarization, with the service links (the broadcast digital audio) using Left Hand Circular Polarization (LHCP) and the TT&C links utilizing Right Hand Circular Polarization (RHCP). While assigned specific center frequencies, bandwidths, and polarizations for the TT&C links, no spacecraft was observed to be exactly on center frequency, and no spacecraft was observed to be perfectly circular in polarization. The exact measured values for frequency and polarization are stored as a time series of data for analysis as part of the satellite characterization objectives of this POC. It is the carriers for these narrowband signals used for TT&C that were utilized for the POC demonstration, as opposed to the wider bandwidth

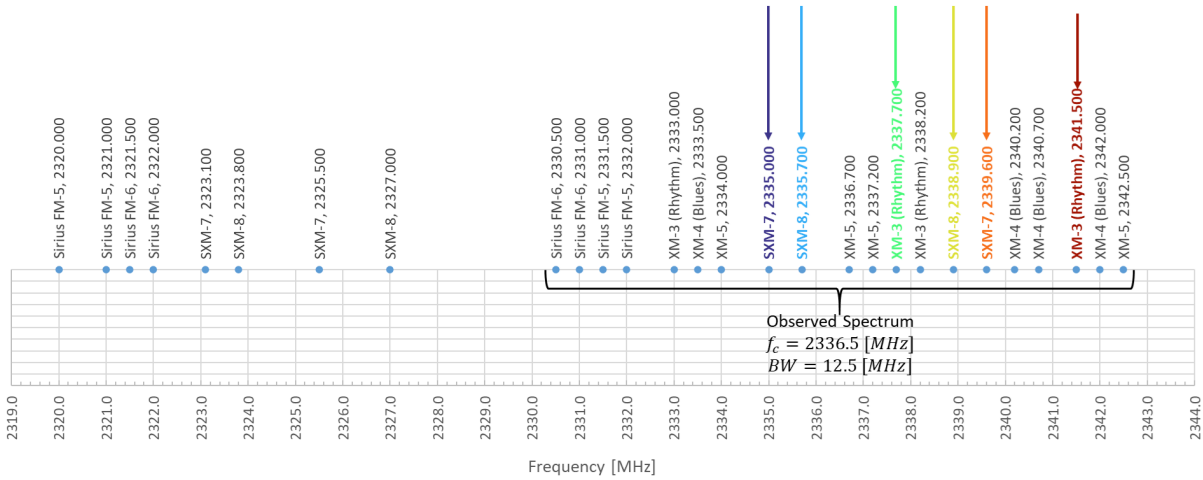

Fig. 11: Channel Assignment for Sirius-XM Constellation TT&C Links.

Phase Shift Keying (PSK) modulated service links, simply to reduce processing requirements and demonstrate that with very narrow carrier measurement alone that useful SDA data can be extracted.

5. RESULTS AND ANALYSIS

The VT-NSI Passive RF testbed is still under development and at the time of writing two of the three antennas for the S-Band differential tracking interferometer have been brought online. Fig.4 shows the differential tracking interferometer that is under development. Only the top portion of this figure is implemented and only with a single baseline (two antennas). While much remains to be installed and brought online, the utility of this particular tracking technique, the data obtained for satellite characterization, and the overall utility of Passive RF in general for SDA applications are shown in the initial results presented in this section.

5.1 Interferometry

A primary objective of this proof of concept demonstration is to obtain sub-arcsecond measurements of satellite motion using Passive RF techniques, in this case specifically using differential interferometric tracking. Fig.12 shows initial results indicating that this requirement has been met and exceeded with sub-arcsecond measurement of the relative motion of the spacecraft achieved. The results in this section are from an approximate two minute data collection window. These figures were produced with GNU Radio's QT GUI blocks, with the dips in the data due to instances of phase wrap in the interferometric phase calculation, which will be rectified in future post processing scripts. The general relative motion trends between the three spacecraft can be seen. The reference satellite was arbitrarily selected to be XM-3, with SXM-7 and SXM-8 selected as the target spacecraft

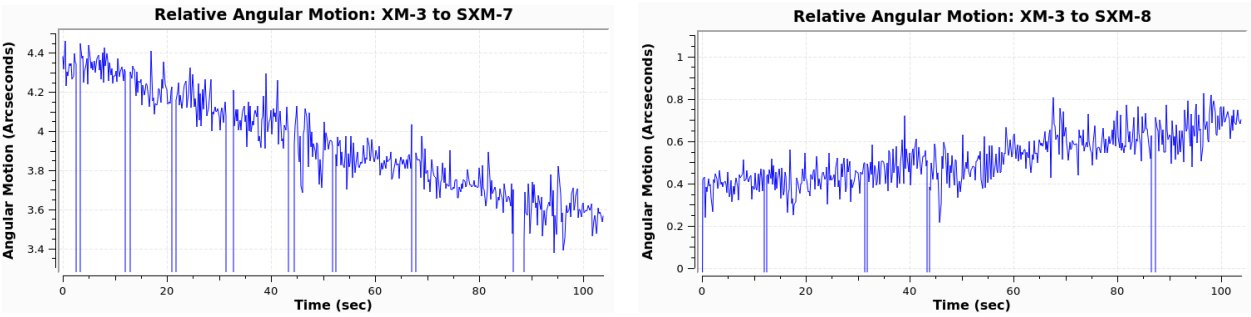

Fig. 12: Angular Motion of XM-3 (Reference) relative to SXM-7 (Target 1, Left) and SXM-8 (Target 2, Right).

5.2 Satellite Characterization

A major secondary objective of this proof of concept is to collect RF data that is useful for satellite characterization, including data suitable for use with AI/ML & RFML techniques. Collection of raw in-phase and quadrature (IQ) digital samples are applicable for RFML applications, when paired with suitable data labelling envisioned to be captured using the SigMF metadata files. The VT-NSI interferometer is now capable of collecting this information, and a data collection campaign has begun, but deployment of RFML techniques are considered future work. Traditional signal processing techniques on the received signals from the Sirius-XM cluster are also relevant for execution of the satellite characterization mission. This section covers initial results where we examine Carrier Frequency Offset (CFO) data as well as polarimetry data.

5.2.1 Carrier Frequency Offset

Consider observation of the RF spectrum when pointing an antenna at the orbital slot for a cluster of three or more spacecraft all operated by the same organization, as is the case with the Sirius-XM cluster. Multiple signals can immediately be observed on air from just a single antenna in the interferometer, see Fig.15. Without additional information, such as the frequency assignment information that was eventually found in open data sources, it is not immediately apparent which spacecraft is emitting which signal. The initial hypothesis was that each signal on air would exhibit different Doppler shift due to the relative motion of the spacecraft. With a stable reference oscillator at the ground station, it is possible to measure the Doppler shift of each signal and map that to a simple orbital model using Two Line Elements and an SGP4 based model for the expected Doppler shift from each satellite. Once each signal is mapped to a specific spacecraft, we can then proceed with the differential interferometric tracking portion of the mission. This was the original reason for exploring the CFO data in detail, but as it turns out, there is much much more information relevant to satellite identification and pattern of life objectives contained within the CFO data alone.

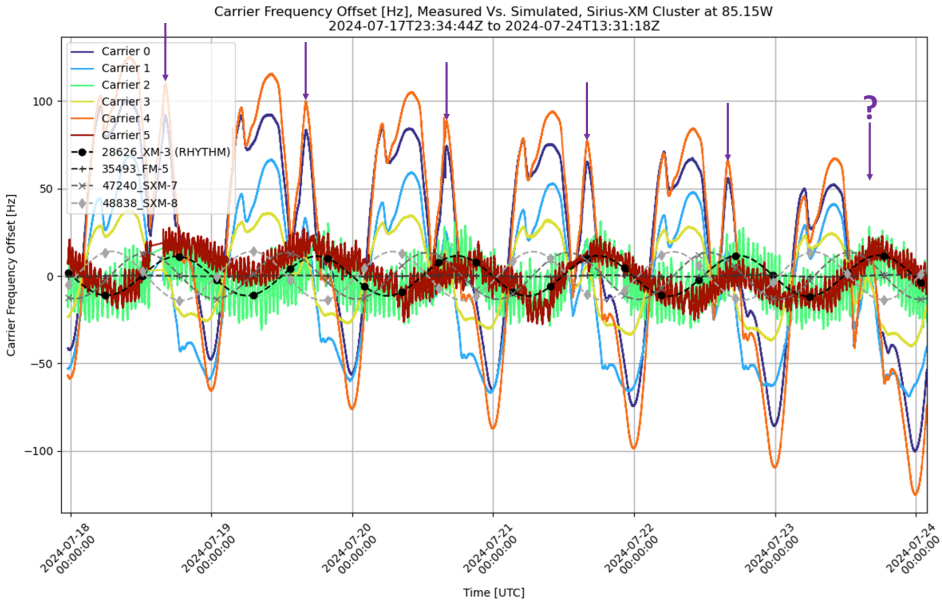

Fig. 13: Carrier Frequency Offset (Doppler) Measurement of Sirius-XM Cluster at 85.15°W Longitude.

Fig.13 shows the results for a 6 sidereal day observation window of the 6 TT&C carriers of interest. The color code of the plot matches the color code used in Fig.11, and shows the solution to the matching of TT&C channel assignments to the individual spacecraft. The dark blue and orange curves map to SXM-7, the light blue and yellow curves map to SXM-8, and the green and brown curves map to XM-3. Nevertheless we still seek to develop a method for confirming this via measurement of the signals for future use when such ground truth data and orbital ephemeris data may not be available. The gray scale plots with icons in the figure shows the expected Doppler shift of the downlinks due to the relative motion of the spacecraft. For the approximate 2.33 GHz operating frequency, the expected Doppler shift to Blacksburg, VA was expected to be no more than about ± 12.5 Hertz, though for four of the signals we see that much

greater excursions were observed. In order to measure this small amount of Doppler shift a stable reference oscillator is required, which is why we elected to use the Trimble Thunderbolt-E GPS Disciplined Oscillators (GPSDO) in the ground station implementation. The frequency stability of these oscillators under locked conditions are measured in parts per *trillion* thus enabling accurate frequency measurement in sub-Hertz regimes in the S-Band frequency allocations.

Some immediately interesting trends are apparent in the dataset. All signals follow an expected periodicity for a sidereal day, 86164.0905 seconds or just under 24 hours. Additionally, we see a slow decay in the general trend of the orange, blue, yellow, and light blue curves. This is also expected from a geosynchronous spacecraft that may be slowly drifting away from its orbit slot assignment. We hoped to find indications of station keeping maneuvers in the dataset, but there are no obvious indications of this and the analysis will continue as more data is collected over longer duration.

The brown and green plots almost perfectly line up with the general Doppler shift trend expected for XM-3. Inspection of Fig.11 confirms that indeed these channels are assigned to XM-3. However, there is a faster periodic oscillation observed in theses curves that has a period of approximately 45 minutes. The faster oscillations appear to line up between both signals, with a positive swing of the green curve occurring at the same time as a positive swing of the brown curve, however the green curve shows a larger amplitude in its deviation. This could be due to a number of factors, and offers a unique signature that would be useful for demonstration of spacecraft identification. The drift is present on two separate TT&C downlinks from the spacecraft, indicating that it is likely occurring in an onboard oscillator that is feeding the RF systems, perhaps due to thermal variations or aging or some combination thereof. This has implications for the state of health of the spacecraft, pattern of life, and satellite identification. XM-3 is also an older spacecraft, launched February 8, 2005 and based on the Boeing BSS-702 bus, and it is likely that these TT&C links are originating from an onboard subsystem that is collecting telemetry data and sending it over the downlinks, with the RF signal originating from onboard the spacecraft. The other four signals on the other hand exhibit some unexpected characteristics that require further scrutiny.

The data for the SXM-7 and SXM-8 spacecraft show frequency deviations on the downlink TT&C signals with much greater deviation than expected due to Doppler shift alone. This is likely due to the composite Doppler shift of both the uplink, in the X-band allocation around 7.0 GHz, and the downlink in S-Band around 2.3 GHz. SXM-7 and SXM-8 are newer spacecraft and are likely utilizing ranging transponders as part of their own station keeping operations, as opposed to the XM-3 spacecraft which matches the expected Doppler shift for a signal originating from the spacecraft itself. A higher fidelity model of the full Sirius-XM system, including the uplink facilities, is currently under development to explore this further.

Finally, interesting changes in the frequency information were also observed from both spacecraft that has implications for pattern of life and are called out with the purple arrows in Fig.13. Consistently for a number of days the data followed a specific pattern, with a noticeable dip then spike in the data just after 1200 UTC. On the last day of observation, the frequency offset did not demonstrate the same spike in the frequency offset, indicated by the purple arrow with the question mark above it. As it is theorized that the measurement is a composite of the uplink and downlink Doppler shift, this may indicate that some action was or was not taken at the ground station facility, again speaking to the pattern of life and offering a test case for event detection type algorithms.

Fig.14 shows a correlation matrix of the measured CFO data. This matrix shows which carriers are associated with other carriers from a frequency measurement perspective. As expected, the correlation score essentially follows the frequency assignments described in Fig.11. This processing tool was developed envisioning a more blind signal search where the question of which signal belongs to which satellite, particularly useful when ground truth is not available.

Of particular interest is the similarities between the SXM-7 (CH0, CH4) and SXM-8 (CH1, CH3) CFO data. Take the first row of the correlation matrix as an example. The correlation score between CH0 and CH4 is 0.99, almost exactly the same as might be expected since both signals are from SXM-7. However, the correlation score from CH0 to SXM-8, CH1 and CH3, while above 90% is not the near perfect score of 99%. The relatively high score is an indicator of the signal similarity, but the non-perfect score is an indicator of the difference between the signals. The similarity may be attributed the fact that both spacecraft are based on the same LSS-1300 bus and are nearly identical, but this is speculation at this point, and there are likely a number of parameters influencing this. On the other hand, the XM-3 channels only show a correlation of 67%, even though we know the signals are coming from the same spacecraft. It is this type of analysis that may be more suited for AI/ML applications to discern these nuances.

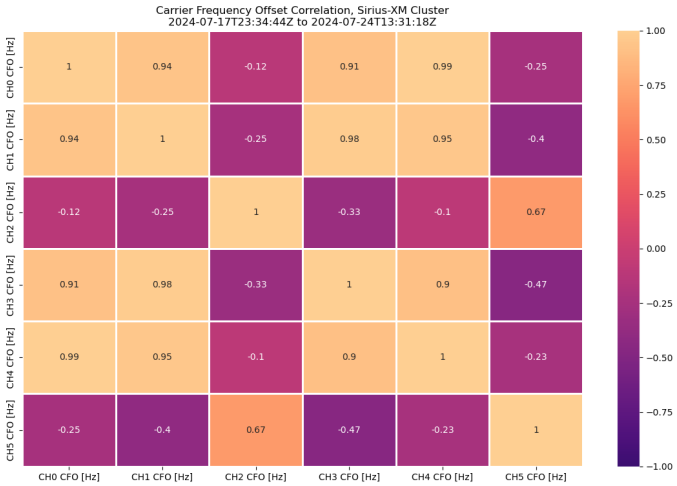

Fig. 14: Carrier Frequency Offset (Doppler) Correlation Matrix of Sirius-XM Cluster at 85.15W Longitude.

5.2.2 Polarimetry

A major secondary objective is to collect RF data that is useful for satellite characterization. Pose estimation, also known as spacecraft attitude, is of interest to the SDA mission. Tracking long term polarization changes of spacecraft downlinks could yield significant data related to the spacecraft pose. Specific features of the polarization metrics may also yield information relevant to spacecraft identification and pattern of life operations. As described in Section 2.2.2, any polarization state can be measured using dual orthogonal linear elements and dual coherent receive chains, a requirement met by the ground station implementation. Only a single ground station's data is needed to conduct the polarimetry, though it is done at all ground stations in the current data pipe-lining process for redundancy purposes. Fig.15 shows the effect of matching polarizations of the received signals. The top left plot shows the spectrum for the

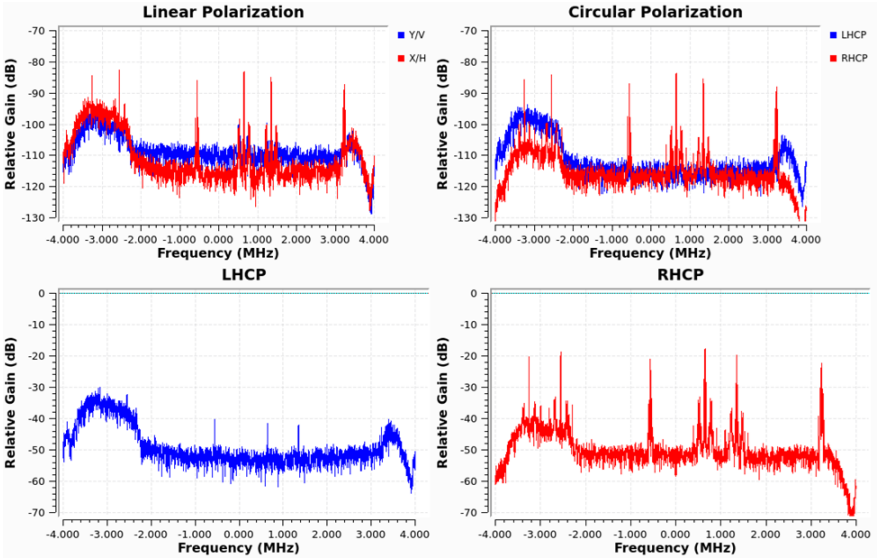

Fig. 15: Polarization Matching of Sirius-XM Cluster at 85.15W Longitude.

linear polarization receive chains. A positive and negative 90 degree phase shift is applied before summing these signals to produce LHCP and RHCP signals, keeping in mind the polarization flip that occurs with prime focus parabolic reflector antennas. This result is shown in the top right figure, with the red curve showing the RHCP IQ stream and the blue curve showing the LHCP IQ stream. The same two plots are broken out in the bottom two plots with LHCP on

the left in blue and RHCP to the right in red to highlight the effects of matching polarization. As can be seen, matching polarizations significantly enhances the SNR of received TT&C signals while suppressing the interfering effect of the wider bandwidth Service links that exist at the same frequency. The polarization matched RHCP TT&C signals are then used to prosecute the differential interferometric tracking operations as well as the CFO measurement operations.

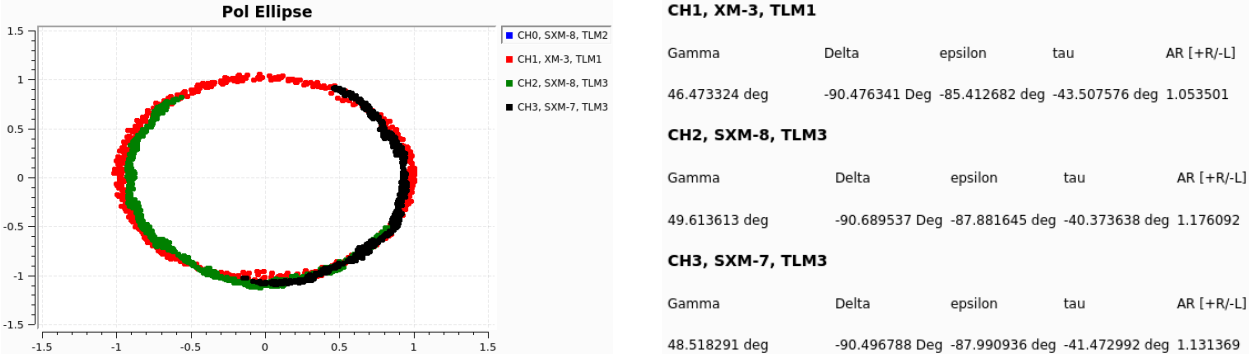

Fig. 16: Graphical representation of a snapshot of the polarization state of the received TT&C links for XM-3, SXM-7, and SXM-8. Polarization Ellipse (left) and values for (γ, δ), (ε, τ), and Axial Ratio (AR) (right).

In addition to matching polarization in order to maximize the SNR of the received signals, a number of metrics can also be measured and logged for later analysis. This is also part of the operations of the system in order to generate datasets useful to the satellite characterization portion of the mission. Fig.16 shows a graphical representation of the incoming polarization of each signal from the three spacecraft of interest. The left figure shows the same polarization ellipse depicted in Fig.5, but with the measured data. If a human operator were monitoring these spacecraft, these types of graphical interfaces, which are continuously updated as the IQ data streams through the processing chain, may be useful sections of an operator console display with changes in the data being quick and obvious to the human eye. Fig.16 (right) shows the key metrics of interest for polarimetry, and are defined in Section 2.2. A snapshot of values for the (γ, δ), (ε, τ), and Axial Ratio are shown. The actual measured values are the (γ, δ) pair of variables, with (ε, τ) and Axial Ratio derived from these measured variables as described by the equations of 2.2.2 and implemented in GNU Radio as shown in Fig.8. In similar fashion to a human operator monitoring a graphical display, one could envision an AI/ML algorithm monitoring these polarimetric data streams and providing event detection warnings to human operators should the state change.

As a final note, consider the Axial Ratio measurements of the three spacecraft (the far right column of the right sub-figure of Fig.16). As with the discussion of the CFO correlation matrix, consider the similarity of the axial ratio for SXM-7 (1.13) and SXM-8 (1.18) compared to each other and compared to the axial ratio of XM-3 (1.05). This slightly higher values of SXM-7 and SXM-8 indicate a slightly less than perfect circular polarization, with a positive value indicating right handed sense. XM-3 on the other hand is closer to a value of 1.0 indicating better circular polarization purity. It is hypothesized that the similarity of the SXM-7 and SXM-8 polarization state may be attributed to both spacecraft utilizing the same bus (and subsystems), which in turn is different than the bus (and subsystems) of XM-3. While this is speculation at this point, this may be another avenue for Machine Learning applications that might not only indicate information concerning satellite identification, but may also be able to provide indications concerning the manufacture of the spacecraft and which bus, or even which generation or variant of bus, is in use.

6. SUMMARY

This paper covers efforts by VT-NSI to develop a Passive RF testbed for Space Domain Awareness as part of the core functionality of the Virginia Tech Ground Station. The initial algorithm developed and deployed is a differential tracking interferometer whose primary purpose is to provide sub-arcsecond tracking data for spacecraft in GEO orbit in the S-Band frequency allocations. In parallel to the tracking operations, the system is also capable of providing information for satellite characterization simultaneously. While the full system is still being implemented, the theory, technical design and implementation, and initial results from a proof of concept, using Sirius-XM, have been presented demonstrating the utility of the techniques, and Passive RF in general, for the SDA Mission.

6.1 Interferometry

The differential tracking interferometer is uniquely suited to the SDA mission. The tracking technique utilized is solely concerned with interferometric phase between the antenna elements of the interferometer and thus does not require long baselines between the antennas,as is usually the case for traditional resolving interferometers used in radio astronomy. The differential processing method, whereby one spacecraft is used as an external reference to cohere the system in order to prosecute and track the signals from a target spacecraft, means the system also does not require exquisite timing and synchronization subsystems, thus lowering overall costs. We have demonstrated the ability to track the Sirius-XM spacecraft at 85.15° West longitude using this technique, with sub-arcsecond resolution.

6.2 Satellite Characterization

Along with the tracking data from the interferometer, the system is also capable of measuring a number of parameters of interest for satellite characterization. The overall design of the system is based on the use of software radio technology and therefore is capable of recording large amounts of raw in-phase and quadrature (IQ) digital samples from each antenna system. These datasets alone, when properly labelled, are immediately useful for Radio Frequency Machine Learning applications. In addition to this a number of metrics are determined using traditional signal processing techniques. Carrier frequency offset, which includes Doppler shift, was measured over an extended 6 day observation window. A number of interesting features exist in that dataset that speak to identification, pattern of life (spacecraft and full system including its ground stations), spacecraft health, maneuver detection, and potentially early warning indicators. Precise measurement of the true center frequency of the spacecraft leads to range-rate information that is planned for incorporation into the tracking model of the system to aid in the orbit determination processing and to extend the concept of the differential tracking interferometer. Polarimetric measurements have also been obtained that again speak to identification, pattern of life, and spacecraft pose, maneuver detection, and potential early warning indicators.

7. FUTURE WORK

7.1 S-Band Interferometer

This paper describes the initial results for a partially built differential tracking interferometer operating in the satellite communications S-Band allocations at 2.20 GHz to 2.40 GHz. Completion of this system is anticipated in the near term future work. The third antenna system will be brought online in order to obtain high resolution angular measurement in azimuth and elevation. Implementation of the full differential tracking algorithm, including the orbital modeling of the reference and target spacecraft is anticipated to map the high resolution angular measurements to real-world orbit determination solutions. Utilization of range-rate information is also expected to be included in the tracking model to extend the current differential tracking interferometer technique and potentially improve the OD solution. Finally, the general data-pipelining process will be refined in order to improve operations and enable smooth collection of tracking data and data for satellite characterization 24/7/365.

7.2 Operating Bands

Expansion of the VT-NSI Passive RF testbed into multiple frequency allocations is part of the expected future work. Moving up in frequency is the likely next step, with interest in X-Band, Ku-Band, and Ka-Band for a number of reasons. As shown in Figure 3, as the frequency of operation is increased, the required baselines for a given target resolution decrease. This relaxes requirements for cohering the systems and has implications for deployable systems. Many designs exist for multi-band antenna feeds as well that can allow for systems to serve multi-band functions while maintaining the requirements for high quality polarimetric measurements. Moving up in frequency introduces equipment known as Low Noise Block downconverters (LNBs) that impart their own phase shifts to the signal. Careful consideration for the implementation of these devices, with strict control or knowledge, of the phase shift they impart is required to maintain the coherency of the system.

7.3 Deployable Systems

RF satellite communication (satcom) stations, refined over decades, offer robust and easily deployable solutions across diverse environments. Their deep manufacturing maturity, combined with larger beamwidths and less stringent pointing precision requirements compared to optical systems, allows for efficient and reliable field deployment. Future work will focus on leveraging these proven RF capabilities to develop systems that prioritize rapid deployment, remote maintenance, and resilience, enabling smooth scaling with minimal logistical effort.

7.4 Identification

Specific Emitter Identification (SEI) leverages hardware imperfections to uniquely identify satellites by their RF signatures. Although SEI has been applied in various domains, its use in satellite identification remains limited [13, 14, 15]. We aim to expand upon existing work by leveraging deep learning on a growing dataset of raw IQ data and spectrograms, while incorporating additional signals and metrics like CFO and polarization discrimination to ground and refine the models.

7.5 Attitude Estimation

Spacecraft orientation can be partially inferred through polarimetry in Passive RF applications. By analyzing signals captured with dual-polarized feeds, Stokes parameters are derived to track variations in linear and circular polarization, which reflect changes in the spacecraft's orientation. We plan to validate this method by comparing our polarimetric pose estimates with publicly available attitude data from targets like the NOAA-GOES series.

8. ACKNOWLEDGEMENTS

This work was performed under the support of KBR and the USSF, Space Systems Command (SSC) AI and Analytics group. The views expressed are solely those of the authors and do not necessarily represent the official policy or position of the U.S. government.

REFERENCES

[1] *Space Doctrine Publication 3-100, Space Domain Awareness*. Accessed July 3, 2024. URL: https://www.starcom.spaceforce.mil/Portals/2/SDP%203-100%20Space%20Domain%20Awareness%20(November%202023)_pdf_safe.pdf.

[2] H. Philip Stahl. "Survey of cost models for space telescopes". In: *Optical Engineering* 49.5 (2010), p. 053005. DOI: 10.1117/1.3430603. URL: https://doi.org/10.1117/1.3430603.

[3] *GNU Radio*. Accessed Jan. 13, 2019. URL: https://www.gnuradio.org/.

[4] *liquid-dsp Software-Defined Radio Signal Processing Library*. Accessed Aug 1, 2024. URL: https://github.com/jgaeddert/liquid-dsp.

[5] William H. Clark IV. "The Importance of Data in RF Machine Learning". Available at http://hdl.handle.net/10919/112668. PhD thesis. Blacksburg, VA: Virginia Tech, Nov. 2022.

[6] Seiichiro Kawase. *Radio Interferometry and Satellite Tracking*. Artech House, 2012. ISBN: 9781608070961.

[7] George W. Swenson Anthony R. Thompson James M. Moran. *Interferometry and Synthesis in Radio Astronomy*. Springer, 2017.

[8] S Kawase and F Sawada. "Interferometric Tracking for Close Geosynchronous Satellites". In: *The Journal of the Astronautical Sciences* 47.2 (1999), pp. 151–167. DOI: https://doi.org/10.1007/BF03546215.

[9] Warren L. Stutzman. *Polarization in Electromagnetic Systems, Second Edition*. Artech House, 2018. ISBN: 9781630811075.

[10] *The White Rabbit Project*. Version. CERN, 2011. URL: https://white-rabbit.web.cern.ch/.

[11] *The Signal Metadata Format (SigMF) Specification*. Version. The GNU Radio Foundation Inc., 2019. URL: https://sigmf.org.

[12] *Virginia Tech Ground Station 2.0*. Accessed Aug 1, 2024. URL: https://github.com/vtgs2.

[13] Ruben Morales-Ferre et al. "Identifying GNSS Signals Based on Their Radio Frequency (RF) Features—A Dataset with GNSS Raw Signals Based on Roof Antennas and Spectracom Generator". en. In: *Data* 5.1 (Feb. 2020), p. 18. ISSN: 2306-5729. DOI: 10.3390/data5010018. URL: https://www.mdpi.com/2306-5729/5/1/18.

[14] Gabriele Oligeri et al. *PAST-AI: Physical-layer Authentication of Satellite Transmitters via Deep Learning*. en. Tech. rep. arXiv:2010.05470. arXiv, Oct. 2020. URL: http://arxiv.org/abs/2010.05470.

[15] Matthew Phelps et al. "Harnessing Speech Recognition for Enhanced Signal Processing of Satellite Communications". In: *GLOBECOM 2023-2023 IEEE Global Communications Conference*. IEEE. 2023, pp. 850–854.